Intramolecular structure and dynamics in computationally designed peptide-based polymers displaying tunable chain stiffness

Nairiti J. Sinha, Yi Shi, Yao Tang, Christopher J. Kloxin, Jeffery G. Saven, Antonio Faraone, Grethe V. Jensen, and Darrin J. Pochan

Phys. Rev. Materials **5**, 095601 — Published 7 September 2021

DOI: 10.1103/PhysRevMaterials.5.095601

Intramolecular structure and dynamics in computationally designed peptide-based polymers displaying tunable chain stiffness

Nairiti J. Sinha,[1,2] Yi Shi,[1] Yao Tang,[1] Christopher J. Kloxin,[1,3] Jeffery G. Saven,[4] Antonio Faraone,[2] Grethe V. Jensen,*[†, 2, 3] Darrin J. Pochan*[1]

[1] Department of Materials Science and Engineering, University of Delaware, Newark, DE 19716.
[2] NIST Center for Neutron Research (NCNR), National Institute of Standards & Technology (NIST), Gaithersburg, MD 20899.
[3] Department of Chemical and Biomolecular Engineering, University of Delaware, Newark, DE 19716.
[4] Department of Chemistry, University of Pennsylvania, Philadelphia, PA 19104.

[†] present address: Danish Technological Institute, Tåstrup, Denmark
*corresponding authors: pochan@udel.edu, gvj@teknologisk.dk

Abstract

Polymers assembled using computationally designed coiled coil *bundlemers* display tunable stiffness via control of inter-bundlemer covalent connectivity as confirmed using small-angle neutron scattering. Neutron spin echo spectroscopy reveals that rigid rod polymers show a decay rate $\Gamma \sim Q^2$ (Q is the scattering vector) expected of straight cylinders. Semi-rigid polymers assembled using bundlemers linked via *4*-armed organic linker show flexible segmental dynamics at mid-Q and $\Gamma \sim Q^2$ behavior at high-Q. The results give insight into linker flexibility-dependent inter-bundlemer dynamics in the hybrid polymers.

Body

The theory of equilibrium and dynamical properties of polymers have been developed and tested against both synthetic and biological materials [1,2]. While most polymer solution studies utilize dynamic light scattering and rheological techniques to investigate macroscopic polymer dynamics, especially in the dilute limit [3], neutron spin echo (NSE) spectroscopy can directly access dynamics at nanometer length scales ($Q > 0.01$ Å^{-1}, Q is the scattering vector) and time

scales of a nanosecond to a few 100 nanoseconds that are especially relevant to biological assemblies and are not accessible to aforementioned characterization techniques [2]. Specifically, NSE spectroscopy combined with small-angle neutron or X-ray scattering yields unique insights into protein and polymer nanostructure and corresponding segmental dynamics at local, inter-monomer distances [2,4]. For example, while theoretical investigations have shown that chain stiffness impacts intra-polymer segmental dynamics [5–7], the underlying inter-monomer segmental dynamics is uniquely accessible to NSE. However, such studies are limited due to the dearth of polymer systems possessing tunable chain stiffness. Some notable examples are investigations of inter-monomer dynamics in linear versus cyclic polymers [7] or polyelectrolyte-salt systems [8,9] that indirectly control chain stiffness by tweaking the polymer architecture or inter-monomer interactions, respectively.

In this letter, we report the impact of inter-monomer linkage on the segmental structure and dynamics of synthetic, supramolecular polymers that display tunable chain stiffness while still having the same monomer unit. Due to the peptidic nature of the monomers, these hierarchical polymer assemblies can form secondary, tertiary and quaternary structure that directly impacts chain stiffness depending on inter-monomer linker type. The results presented in this article also point to the uniqueness of biopolymers in forming such 1D assemblies with disparate chain stiffness.

Specifically, the polymers are constructed via a novel assembly pathway involving hybrid physical-covalent connections between cylindrical, peptidic assembly units, called bundlemers. Bundlemers are computationally designed coiled coils of four identical peptides whose peripheral interactions are readily tuned by amino acid sequence modification such that the resulting bundlemers can form target nanostructures, from non-natural 2D lattices to soluble patchy colloidal particles [10,11]. Using the transmission electron microscopy characterization technique, we have shown in a previous publication that 1D polymers of bundlemers of varying chain stiffness can be synthesized using the facile thiol-Michael *click* chemistry reaction between bundlemers end-functionalized with thiol and maleimide [12,13]. This assembly pathway yields sequence-defined, hierarchical polymers wherein the bundlemers function as supramolecular "monomer" building blocks held together by desired organic linkers. The control of chain stiffness in the polymers is achieved by changing the linker type between the neighboring bundlemers; a

direct one-to-one linkage of bundlemers ends with short, hydrocarbon linkers resulted in formation of ultra-stiff, rigid rod-like polymers, whereas linkage of bundlemer ends via the short arms of an added, multifunctional organic crosslinker resulted in semi-rigid polymers [12]. Thus, even though the chains are constructed with the same bundlemer building block, the two polymers are unique where the former is essentially a straight cylinder and the latter mimics the description of a broken-rod model [14] (see **Fig. 1 (A) & (B),** assembly details are given in *supplementary information*).

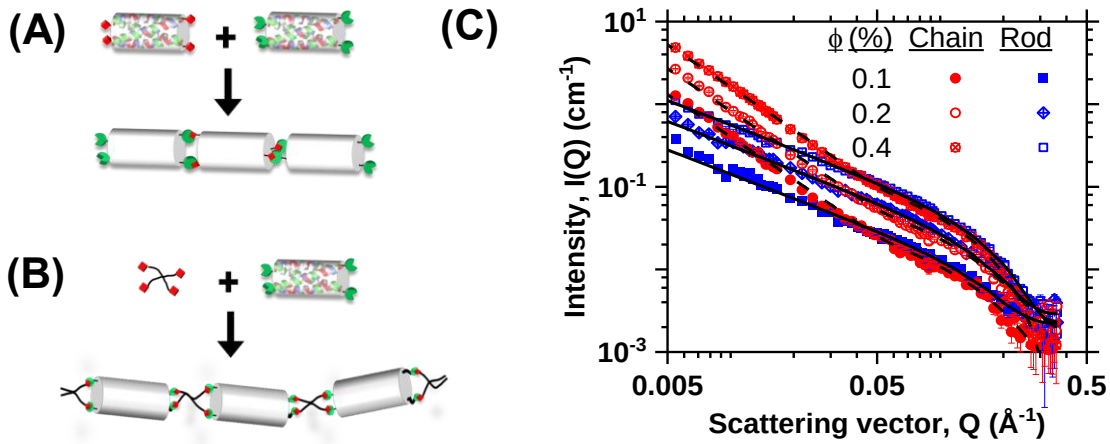

Fig. 1: Schematic of hybrid physical-covalent assembly of polymers formed via **(A)** direct linkage and **(B)** flexible small molecular linker. The bundlemers are depicted as grey cylinders overlaying the ribbon diagram, where each of the four peptides that constitute the bundlemer have the sequence DEEIRRMAEEIRKMAERIKQMAEQIYKEA-NH_2. The N-terminus of the peptide is either functionalized with maleimide (red diamonds, **Peptide_A)** or thiol (green, cut circles, **Peptide_B)** functional groups. The thiol-Michael click reaction between **Peptide_A** and **Peptide_B** or **Peptide A** and a tetrathiol functional small molecule (PETMP) results in the formation of rigid rod-like polymers or semi-rigid polymers, respectively. **(C)** SANS data for a concentration series of the semi-rigid polymers ("Chain", red circles) and rigid rod-like polymers ("Rod", blue squares) dissolved in deuterium oxide (D_2O) and 50 x 10^{-3} mol/L sodium chloride (NaCl). The concentration of polymer is reported in volume fraction, Φ. The solid and dashed black lines are the corresponding fits to a straight cylinder and flexible cylinder form factor models, respectively. Error bars represent $\pm 1\sigma$ (standard deviation).

For this study, we have utilized *homo*polymers where both rigid rods and semi-rigid chains were constructed using the same bundlemer-forming peptides having an amidated C-terminus and either a maleimide-functionalized N-terminus (via addition of N-carboxypropyl maleimide, **Peptide_A**) or thiol-functionalized N-terminus (via addition of a cysteine, **Peptide_B**). To construct rigid rods, bundlemers formed from the self-assembly of **Peptide_A** were reacted with bundlemers of **Peptide_B** (refer to **Fig.1 (A)**), whereas the construction of semi-rigid chains

involved reaction of **Peptide_A** bundlemers with pentaerythritol tetrakis(3-mercaptopropionate) (PETMP) (refer to **Fig. 1 (B)**). Throughout this paper, SANS and NSE results extracted from measured data are plotted using statistically averaged data points with error bars representing ±1σ (standard deviation) [15,16], and best fits were chosen by the method of least-squares having the lowest reduced chi-squared values (all equations and fit parameters are summarized in *supplementary information*) [16,17].

Previously, the structure and solution properties of a single bundlemer have been characterized using small-angle neutron scattering (SANS), revealing cylindrical dimensions of ≈ 20 Å diameter and ≈ 40 Å length [11]. Here, we briefly discuss the structural characterization of assembled polymers in solution that was performed using SANS. For a dilute solution of isotropically scattering monodisperse particles, the scattering intensity profile $I(Q)$ is described by [18],

$$\mathrm{I(Q)} = \mathrm{nV_p^2(\rho_p - \rho_s)^2\ P(Q)},\ \ldots\ (1)$$

where n is the number density of scatterers having a volume V_p and a scattering length density ρ_p dispersed in a solvent with a scattering length density ρ_s. The shape and size of the scatterers is captured in the form factor, $P(Q)$, averaged over all possible particle orientations.

The solution conditions for SANS measurements were optimized to ensure form factor-like scattering of non-interacting polymers over the entire probed Q-range. Specifically, sodium chloride (NaCl) salt was added to the polymer solution to screen any local repulsion between the polymers that had resulted in a correlation hole in the scattering curves in our previous investigations [12,13]. The SANS data for a concentration series of the two polymer types in 50 x 10^{-3} mol/L sodium chloride are shown in **Fig. 1 (C).** The curves confirm the distinct nanostructure of the rigid rods versus semi-rigid chains even while both polymers are constituted by the same bundlemer unit. Here, the rigid rods and semi-rigid chains have an identical feature at $Q \approx 0.1$ Å^{-1} corresponding to a circular cross-section of the assembled polymers. For $Q < 0.1$ Å^{-1}, the rigid rod system shows a $I \sim Q^{-1}$ dependence in the entire probed Q-range due to its rod-like structure. Thus, the rigid rods were modeled using a cylinder form factor that we have also used previously [13] (equations for form factor models are given in *supplementary information*). Fit results show that the rigid rods have a radius of 10.6 (± 0.4) Å and length which is beyond the range of the SANS measurements (greater than 1250 Å). In contrast, the semi-rigid chains show a

scattering fingerprint characteristic of Kratky-Porod worm-like chains, wherein the $I \sim Q^{-1}$ dependence in intermediate-Q deviates to a steeper $I \sim Q^{-1.73}$ scaling for $Q < Q^*$ where $Q^* \approx 0.04$ Å^{-1} [19,20]. Therefore, the semi-rigid chains were modeled using the flexible cylinder form factor, which yields a 10.0 (± 0.2) Å radius, a 71.0 (± 1.0) Å Kuhn length (k_L), and an overall chain length beyond the range of the SANS measurements. It is important to note that both polymer types are inherently polydisperse in length due to step growth polymerization kinetics of Thiol-Michael *click* chemistry reaction. This aspect of their length distribution has been proven previously using Transmission Electron Microscopy (TEM) [12,13], and cannot be captured by SANS measurements since scattering intensity is sensitive to larger species in solution (see eq.(1)).

The SANS fits corroborate our previous findings that both rigid rods and semi-rigid chains have the same cross-section as that of a single bundlemer unit, which is expected for end-to-end polymerized bundlemers described by schematic in **Fig. 1A** and **1B** [12]. Specifically, for the semi-rigid chains, a persistence length $l_p = k_L/2$ = 35.4 Å is calculated using the fitted value for the Kuhn length, and is approximately equal to the length of a single bundlemer unit. However, the rigid rods have large persistence lengths that are beyond the Q-range probed here. Thus, while both polymer types herein have similar mass per unit length, the rigid rod polymers exhibit at least two orders of magnitude larger persistence length than the semi-rigid chains. This is an important result since it is well-established that 1D materials have persistence lengths that generally scale linearly as their mass per unit length [12,21]. Also, the contour length of the organic linkers between neighboring bundlemers within the rigid rod polymers is half the length of a fully stretched PETMP linker within the semi-rigid chains. Therefore, SANS measurements allude to an increase in chain flexibility in semi-rigid chains at inter-bundlemer length scales in comparison to the rigid rods which can be attributed to the presence of the organic PETMP crosslinker between bundlemers in the former polymer type. These SANS results are consistent with our previous TEM studies of the two bundlemer-based polymers [12].

Since concentration dependent effects are not observed for either of the polymer types, interparticle correlations are considered negligible. Thus, segmental dynamics of individual polymers dominate in this Q-range. NSE spectroscopy measurements was used to probe these inter-bundlemer dynamics within the two types of polymer chains. The extracted intermediate

scattering function, $I(Q,t)$, from the neutron echo data was fitted using a single stretched exponential function which is characteristic of intra-polymer dynamics [22],

$$\frac{I(Q,t)}{I(Q,0)} = \exp[-(\Gamma(Q)\ t)^{\beta}] \quad . \quad \ldots (2)$$

In this expression, β is the stretching exponent and Γ is the first cumulant of dynamic correlations, also called the decay rate, which is a function of scattering vector, Q. Here, we briefly discuss the dynamical theories applicable to the polymers [2]. For $QR_G < 1$, where R_G is the polymer radius of gyration, length scales beyond the over-all size of the polymer are probed and macroscopic diffusion of center-of-mass of the polymers dominate. This yields classic free-diffusion and $\Gamma = \bar{D}\ Q^2$ where $\bar{D}$ is the mean diffusion coefficient of the polymer and the stretching exponent $\beta = 1$. Since the bundlemer-based polymers have a large aspect ratio, are polydisperse (as discussed above due to the step-growth polymerization kinetics), and can form fractal aggregates [13], dynamic light scattering measurements do not yield useful information about inter-bundlemer segmental dynamics and were not used to probe low-Q dynamics in this study.

In the regime $QR_G > 1$, intra-polymer dynamics dominate and β and Γ depend on the length scales and corresponding chain stiffness [5,7]. We are specifically interested in the dynamic regime $Qb \ll 1$ for polymers having rod-like segments of length b, where intra-polymer Rouse-($\beta = 1/2, \Gamma \sim Q^4$) or Zimm-modes ($\beta = 2/3, \Gamma \sim Q^3$) have been reported for polymers in melt and in solution respectively [2,6,23]. Based on the SANS measurements, we therefore focus our Q-range to $1 < Qb < 2\pi$, where $b = 37$ Å is the length of a bundlemer unit. Importantly, for stiff 1D assemblies, such as the polymers probed in this study, Zilman and Granek have derived a stretching exponent $\beta = 3/4$ and segmental decay rate dependence $\Gamma \sim Q^{8/3}$ due to thermally accessible bending fluctuations along rod-like segments [24]. Such bending modes have been observed in stiff polymers and 1D assemblies like worm-like micelles and self-assembled peptidic hydrogels [25,26]. Finally, we discuss the case of the straight cylinder that is expected to display free diffusion dynamics with $\beta = 1$, $\Gamma = DQ^2$ over the entire Q-range. In this case, the diffusion coefficient, $D = \frac{D_{\parallel} + 2D_{\perp}}{3}$ depends on the parallel ($D_{\parallel}$) and perpendicular ($D_{\perp}$) components of diffusion coefficient, as well as a rotational component (D_{θ}) which was derived by Broersma [27,28], and is sensitive to the rod concentration regime as described by Doi and Edwards [29–31]. Importantly, at large scattering vectors that are accessible to NSE, i.e., when

$Qb \approx 2\pi$, segmental dynamics within a flexible polymer can be used to extract an apparent monomer diffusion coefficient within the polymer, $D_{mon} = \frac{\Gamma}{Q^2}$ [2,32].

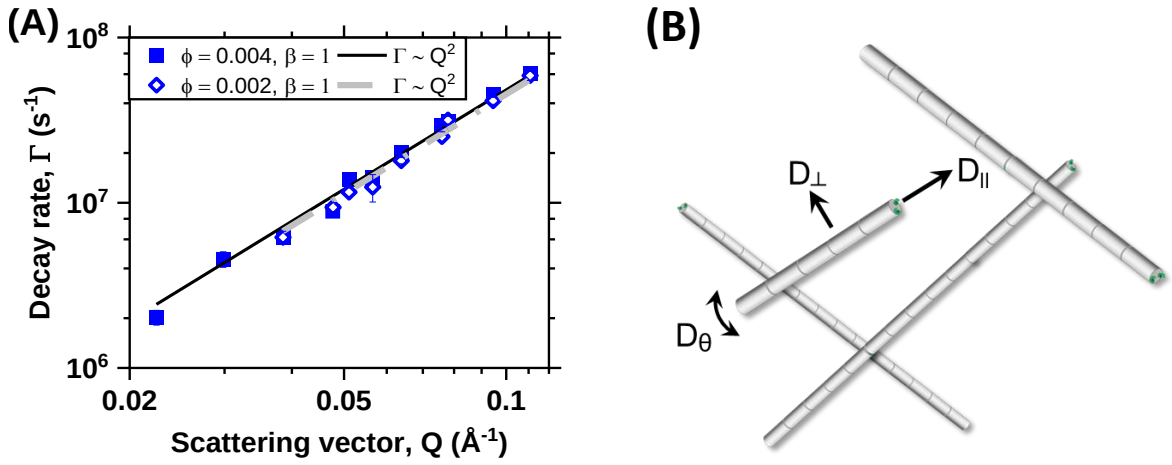

Fig. 2: (A) Neutron spin echo (NSE) data and scaling-law fits for rigid rod-like polymers. Measurements were performed on freshly prepared samples containing a two different volume fraction of polymers, Φ, in deuterium oxide with 50 x 10^{-3} mol/L sodium chloride at 22ºC. The black solid and grey dashed line are fits to free diffusion dynamics. **(B)** Schematic of short rods diffusing in a network of long rods. Components of the diffusion coefficient D are indicated in the parallel ($\parallel$), perpendicular ($\perp$) and rotational (θ) directions. Error bars representing $\pm 1\sigma$ (standard deviation).

We first discuss the results for the rigid rod polymers and compare them with semi-rigid polymers later in the paper. The measured intermediate scattering function was fit to the single exponential free diffusion equation and displayed a single dynamic regime in the entire probed Q-range (see *supplementary information* **Fig. S3)**. The extracted results for decay rate Γ versus scattering vector Q for rigid rods are plotted on a log-log scale for two concentrations in **Fig. 2A** . The diffusion coefficient extracted for the rigid rod-like polymers (RR) were similar, with $\bar{D}_{RR\,\{\varphi=0.004\}} = 4.8\ (\pm\ 0.1)\ \text{x}\ 10^{-11}\ m^2/s$ and $\bar{D}_{RR\,\{\varphi=0.002\}} = 4.5\ (\pm\ 0.1)\ \text{x}\ 10^{-11}\ m^2/s$. One can use Broersma's equations for freely diffusing rods [27,28] to calculate the apparent aspect ratio of an equivalent dilute solution of monodisperse rods using the measured total diffusion coefficient and measured cross-section, which is ≈ 10.5 (apparent length $L_{app} \approx 22$ nm) with $\bar{D}_\parallel/3$ contributing to ≈ 62 % of this value (see *supplementary information* for calculation). From our previous studies [12,13], we know that the rods have polydisperse lengths. Consequently, $\bar{D}_{RR}$ is the average of the corresponding contributions by individual rod lengths. Thus, NSE spectroscopy indicates that the rigid rod-like polymers diffuse like straight stiff cylinders wherein the faster

diffusing short rods contribute to the *I (Q, t)* more than long rods which form a network of sluggishly diffusing rods in the background, **Fig. 2B.** Also, the rotation diffusion coefficient $\bar{D}_\theta$ can be neglected since it happens over time scales of a few microseconds which is beyond the scope of NSE spectroscopy measurements (see *supplementary information* for calculations).

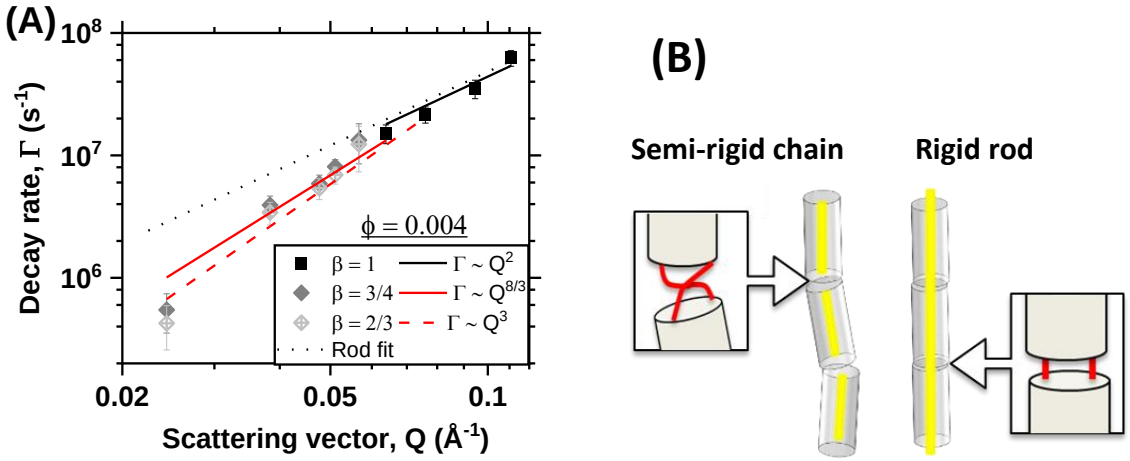

Fig. 3: Neutron spin echo (NSE) data and scaling-law fits for **(A)** semi-rigid polymers. Measurements were performed on freshly prepared samples containing a Φ=0.004 volume fraction of polymers in deuterium oxide with 50 x 10^{-3} mol/L sodium chloride at 22ºC. Error bars representing ±1σ (standard deviation). **(B)** A schematic of the rigid rod-like (right) and semi-rigid chain-like (left) polymers, where the hydrophobic core is illustrated in yellow. This core propagates through the axis of the rigid rods and is segmented in the semi-rigid chains due to differences in type of linkers (red, insets).

In contrast, the *I(Q,t)* data for the semi-rigid (SR) chains did not follow the free diffusion description for the entire *Q*-range, but instead exhibited two distinct dynamical regimes that were *Q*-dependent, **Fig. 3A** (see *supplementary information* for model details). In the high-*Q* regime, fits to *I (Q, t)* using $\beta = 1$ yielded a satisfactory $\Gamma \sim Q^2$ scaling. The extracted diffusion coefficient in this *Q*-regime was $D_{SR} = 4.4\ (\pm\ 0.2)$ x $10^{-11} m^2/s$ which can be attributed to the constituent bundlemer diffusion manifesting at high-*Q*. In the intermediate-*Q* regime, which corresponds to inter-bundlemer distances, a systematic deviation from $log\left(\frac{I(Q,t)}{I(Q,0)}\right) \sim -D_{SR}Q^2t$ behavior (i.e. free diffusion relation) to $log\left(\frac{I(Q,t)}{I(Q,0)}\right) \sim -(D'Q^{\frac{2}{\beta}}t)^\beta$ behavior was recorded where $\beta < 1$ and *D'* is an apparent segmental diffusion coefficient (see **Fig. S4** and **Fig. S5** in *supplementary information*). This deviation indicates that additional segmental dynamics are contributing to the *I (Q, t)* of the semi-rigid chains in this *Q*-regime. Both thermally activated bending dynamics described by Zilman-Granek model with β = ¾ and flexible chain dynamics impacted by intrachain viscosity

described by the Zimm model with $\beta = 2/3$ yielded superior fits to the *I (Q, t)* data in this *Q*-regime. However, due to the narrow *Q*-range accessible to the NSE instrument as well as dilute polymer concentrations, we could not measure low-*Q* data points with good statistics to definitively quantify the segmental dynamics in this *Q*-regime. Nevertheless, from the NSE data we conclude that two *Q*-dependent dynamical regimes exist and diverge at a critical scattering vector $Q^* \approx 0.06\ \text{Å}^{-1}$ which corresponds to a length scale that is comparable to the semi-rigid chain's Kuhn length, k_L**.**

Comparison of the dynamics of rigid rods and semi-rigid polymers yields interesting insights. Firstly, since the *I (Q, t)* data is skewed towards fast dynamics of shorter rods in the rigid rod samples, similarity of decay rate at high-*Q* results specifically for given polymer samples under probed solution conditions. Secondly, in the intermediate-*Q* regime, i.e. $Q < Q^*$, the decay rate Γ_{SR} and, consequently, the apparent diffusion coefficient ($\frac{\Gamma_{SR}}{Q^2}$) for the semi-rigid chains is less than that of rigid rods (Γ_{RR}) (comparing the rod and chain fits in **Fig. 3A**). We infer that the smooth linear architecture of shorter rods enables faster diffusion whereas, steric costs of bending result in the slower inter-bundlemer diffusion in the longer and locally entangled semi-rigid chains in this *Q*-range. Finally, fits for the amplitude *I(Q,0)* to the intermediate scattering function yield useful insight into dynamics within the two polymer systems (see **Table S10** in *supplementary information*). Ideally, if all fast dynamics in the system is captured, *I(Q,0)* = 1 [2]. The fitted values indicate that NSE spectroscopy successfully captures all fast dynamics within the rigid rod polymers ($\langle I(Q,0)\rangle_{RR}$ = 0.96 ± 0.02). However, all fast dynamics are not accessible to NSE spectroscopy in the semi-rigid polymers ($\langle I(Q,0)\rangle_{SR}$ = 0.88 ± 0.04) which may be attributed to the presence of internal dynamics within the semi-flexible polymer due to the flexibility of the PETMP linker.

The absence of inter-bundlemer bending dynamics in rigid rod-like polymers in NSE spectroscopy studies indicate that inter-bundlemer bending modes are constrained in these polymers. These results combined with SANS measurements corroborate our previous studies wherein we showed that the rigid rod-like polymers have exceptionally long persistence lengths of greater than a micrometer [12]. We suspect that hydrophobic contacts between bundlemer cores and α-helical hydrogen bonds between neighboring bundlemers can be facilitated by the short inter-bundlemer linker resulting in the formation of quaternary structure in rigid rod-like

polymers that can further suppress bending dynamics (see schematic in **Fig. 3B**). In contrast, NSE and SANS investigations of the semi-rigid chain-like polymers indicate that segmental dynamics are activated at inter-bundlemer length scales, which can be ascribed to bending at the PETMP linker junction. In this case, the 'crossed' geometry of the PETMP molecule may inhibit further interactions between bundlemers (**Fig. 3B**). Therefore, this study of tunable supramolecular polymer systems constructed using the same macromolecular building block shows that linker type intimately impacts bundlemer chain structure as well as dynamics at the nanoscale.

We have shown that NSE spectroscopy combined with SANS measurements yields unique and hitherto inaccessible information of the impact of purely the inter-monomer linker type on the persistence length and resulting chain stiffness of the exotic peptidic assemblies. In the future, the unique hybrid assembly pathway will enable the exploration of the impact of solvent quality and inter-bundlemer interactions via charge pattern on dynamics of new self-assembled 1D and 2D architectures.

Acknowledgements: This manuscript was prepared under cooperative agreement #370NANB17H302 from National Institute of Standards and Technology (NIST), U.S. Department of Commerce. We acknowledge the support of the NIST, U.S. Department of Commerce in providing the neutron research facilities used in this work. Access to v SANS was provided by the Center for High Resolution Neutron Scattering (CHRNS), a partnership between the National Institute of Standards and Technology and the National Science Foundation under Agreement No. DMR-1508249. Support for peptide design, synthesis, purification, and bundlemer rod formation was provided by the Department of Energy, Office of Basic Energy Sciences, Biomolecular Materials Program under grant No. DE-SC0019355 and DE-SC0019282. Samples were prepared for experiments at the NIST/IBBR Biomolecular Labeling Laboratory.

Disclaimer: The statements, findings, conclusions and recommendations are those of the authors and do not necessarily reflect the view of NIST or the U.S. Department of Commerce. Certain commercial equipment, instruments, materials, suppliers and software are identified in this paper to foster understanding. Such identification does not imply recommendation or endorsement by the NIST, nor does it imply that the materials or equipment identified are necessarily the best available for the purpose.

References:

[1] P. G. de Gennes and T. A. Witten, *Scaling Concepts in Polymer Physics*, Phys. Today **33**, 51 (1980).

[2] B. Ewen and D. Richter, *Neutron Spin Echo Investigations on the Segmental Dynamics of Polymers in Melts, Networks and Solutions*, in *Neutron Spin Echo Spectroscopy Viscoelasticity Rheology* (Springer Berlin Heidelberg, Berlin, Heidelberg, 1997), pp. 1–129.

[3] T. Norisuye, *Semiflexible Polymers in Dilute Solution*, Prog. Polym. Sci. **18**, 543 (1993).

[4] Y. Liu, *Short-Time Dynamics of Proteins in Solutions Studied by Neutron Spin Echo*, Curr. Opin. Colloid Interface Sci. **42**, 147 (2019).

[5] L. Harnau, R. G. Winkler, and P. Reineker, *Influence of Stiffness on the Dynamics of Macromolecules in a Melt*, J. Chem. Phys. **106**, 2469 (1997).

[6] L. Harnau, R. G. Winkler, and P. Reineker, *Dynamic Structure Factor of Semiflexible Macromolecules in Dilute Solution*, J. Chem. Phys. **104**, 6355 (1996).

[7] V. Arrighi, S. Gagliardi, F. Ganazzoli, J. S. Higgins, G. Raffaini, J. Tanchawanich, J. Taylor, and M. T. F. Telling, *Effect of Chain Length and Topological Constraints on Segmental Relaxation in Cyclic PDMS*, Macromolecules **51**, 7209 (2018).

[8] J. Hayter, G. Janninck, F. Brochard-Wyart, P. G. de Gennes, and P. G. de Gennnes, *Correlations and Dynamics of Polyelectrolyte Solutions*, J. Phys. Lett. **41**, 451 (1980).

[9] V. M. Prabhu, *Counterion Structure and Dynamics in Polyelectrolyte Solutions*, Curr. Opin. Colloid Interface Sci. **10**, 2 (2005).

[10] H. V. Zhang, F. Polzer, M. J. Haider, Y. Tian, J. A. Villegas, K. L. Kiick, D. J. Pochan, and J. G. Saven, *Computationally Designed Peptides for Self-Assembly of Nanostructured Lattices*, Sci. Adv. **2**, e1600307 (2016).

[11] M. J. Haider, H. V. Zhang, N. Sinha, J. A. Fagan, K. L. Kiick, J. G. Saven, and D. J. Pochan, *Self-Assembly and Soluble Aggregate Behavior of Computationally Designed Coiled-Coil Peptide Bundles*, Soft Matter **14**, 5488 (2018).

[12] D. Wu, N. Sinha, J. Lee, B. P. Sutherland, N. I. Halaszynski, Y. Tian, J. Caplan, H. V. Zhang, J. G. Saven, C. J. Kloxin, and D. J. Pochan, *Polymers with Controlled Assembly and Rigidity Made with Click-Functional Peptide Bundles*, Nature **574**, 658 (2019).

[13] N. J. Sinha, D. Wu, C. J. Kloxin, J. G. Saven, G. V Jensen, and D. J. Pochan, *Polyelectrolyte Character of Rigid Rod Peptide Bundlemer Chains Constructed via Hierarchical Self-Assembly*, Soft Matter **15**, 9858 (2019).

[14] J. B. Lagowski, J. Noolandi, and B. Nickel, *Stiff Chain Model—Functional Integral Approach*, J. Chem. Phys. **95**, 1266 (1991).

[15] S. R. Kline, *Reduction and Analysis of SANS and USANS Data Using IGOR Pro*, J. Appl. Crystallogr. **39**, 895 (2006).

[16] R. T. Azuah, L. R. Kneller, Y. Qiu, P. L. W. Tregenna-Piggott, C. M. Brown, J. R. D. Copley, and R. M. Dimeo, *DAVE: A Comprehensive Software Suite for the Reduction, Visualization, and Analysis of Low Energy Neutron Spectroscopic Data*, J. Res. Natl. Inst. Stand. Technol. **114**, 341 (2009).

[17] M. Doucet, J. H. Cho, G. Alina, J. Bakker, W. Bouwman, P. Butler, K. Campbell, T. Cooper-Benun, C. Durniak, L. Forster, M. Gonzales, R. Heenan, A. Jackson, S. King, P. Kienzle, J. Krzywon, T. Nielsen, L. O'Driscoll, W. Potrzebowski, R. Ferraz Leal, P. Rozycko, T. Snow, and A. Washington, *SasView Version 5.0*, (2019).

[18] P. Lindner and T. Zemb, *Neutron, X-Rays and Light. Scattering Methods Applied to Soft Condensed Matter*, Mater. Today **5**, 38 (2002).

[19] J. S. Pedersen and P. Schurtenberger, *Scattering Functions of Semiflexible Polymers with and without Excluded Volume Effects*, Macromolecules **29**, 7602 (1996).

[20] W.-R. Chen, P. D. Butler, and L. J. Magid, *Incorporating Intermicellar Interactions in the Fitting of SANS Data from Cationic Wormlike Micelles*, Langmuir **22**, 6539 (2006).

[21] D. Boal, *Mechanics of the Cell*, Vol. 100 (Cambridge University Press, Cambridge, 2012).

[22] D. Richter and B. Ewen, *Dynamical Scaling in Polymer Solutions*, in *Scaling Phenomena in Disordered Systems*, edited by R. Pynn and A. Skjeltorp (Springer US, Boston, MA,

1991), pp. 491–506.

[23] M. Benmouna, A. Z. Akcasu, and M. Daoud, *Effect of Stiffness on the First Cumulant and Polymer Dimensions in Solution*, Macromolecules **13**, 1703 (1980).

[24] A. G. Zilman and R. Granek, *Undulations and Dynamic Structure Factor of Membranes*, Phys. Rev. Lett. **77**, 4788 (1996).

[25] F. Nettesheim and N. J. Wagner, *Fast Dynamics of Wormlike Micellar Solutions*, Langmuir **23**, 5267 (2007).

[26] M. C. Branco, F. Nettesheim, D. J. Pochan, J. P. Schneider, and N. J. Wagner, *Fast Dynamics of Semiflexible Chain Networks of Self-Assembled Peptides*, Biomacromolecules **10**, 1374 (2009).

[27] S. Broersma, *Viscous Force Constant for a Closed Cylinder*, J. Chem. Phys. **32**, 1632 (1960).

[28] S. Broersma, *Rotational Diffusion Constant of a Cylindrical Particle*, J. Chem. Phys. **32**, 1626 (1960).

[29] M. Doi, *Rotational Relaxation Time of Rigid Rod-like Macromolecule in Concentrated Solution*, J. Phys. **36**, 607 (1975).

[30] M. Doi and S. F. Edwards, *Dynamics of Rod-like Macromolecules in Concentrated Solution. Part 1*, J. Chem. Soc. Faraday Trans. 2 **74**, 560 (1978).

[31] M. Doi and S. F. Edwards, *Dynamics of Rod-like Macromolecules in Concentrated Solution. Part 2*, J. Chem. Soc. Faraday Trans. 2 **74**, 918 (1978).

[32] L. K. Nicholson, J. S. Higgins, and J. B. Hayter, *Dynamics of Dilute Polymer Solutions*, Macromolecules **14**, 836 (1981).

[33] See Supplemental Material at [*URL will be inserted by publisher*] for description of peptide synthesis and assembly, scattering data analyses and models and tables of corresponding fit parameters.